Bulletin of Volcanology (2024) 86:90
https://doi.org/10.1007/s00445-024-01778-w

RESEARCH ARTICLE

Run-out distance of initially fluidized, collapsing granular columns with different aspect ratios: constraints and volcanological implications from experiments and 2D incompressible simulations

Alvaro Aravena[1,2,3] · Laurent Chupin[4] · Thierry Dubois[4] · Olivier Roche[2]

Received: 21 August 2024 / Accepted: 24 October 2024

Abstract
We investigate granular flows generated by the collapse of an initially fluidized column into a horizontal channel in order to evaluate the factors controlling the efficiency of fluidization in increasing the run-out distance of pyroclastic density currents. This configuration is analogous to flows generated by the collapse of volcanic domes or lava flow fronts. We use an incompressible two-phase numerical model able to simulate dam-break experiments, and we compare the numerical results with experimental data. This model permits us to describe depth-dependent variations of flow properties and the effect of pore pressure on the rheology of the granular material. We show that the interplay between timescales of column collapse and of flow front propagation plays a primary role in determining the effective influence of fluidization on run-out distance. For columns with a high aspect ratio (i.e., initial height/initial width), the collapse velocity decreases abruptly after reaching its peak, a significant portion of the collapse has occurred when the flow front has travelled a long distance from the reservoir and, importantly, the decrease of basal pore pressure with time in the reservoir translates into a reduced velocity of the granular material entering into the propagation channel during final phases of collapse. Thus, at some point, the collapsing material is not able to significantly affect the flow front dynamics. This behaviour contrasts with that of low aspect ratio collapsing columns. These results are consistent with complementary analogue experiments of high-aspect-ratio collapsing columns, which show that the granular material at the front of the deposit originates from lower levels of the column. Comparison with new experimental data also reveals that the effective pore pressure diffusion coefficient in the propagating flow is an increasing function of column height, and it can be considered as proportional to a weighted average of flow thickness during propagation. This is consistent with experiments on static defluidization columns, but had not been tested in dam-break experiments until this study. Considering this type of dependency, under our experimental and simulation conditions, the non-dimensional run-out distance presents a relative maximum for initial aspect ratios between 1 and 2, and beyond this critical range, the non-dimensional run-out distance decreases abruptly.

Keywords Fluidization · Dam-break experiments · Pore pressure diffusion coefficient · Pyroclastic density currents

Introduction

Pyroclastic density currents (PDCs) are high-speed flows composed of pyroclasts, lithic fragments and gas that propagate laterally on flanks of volcanoes due to the effect of gravity (Druitt 1998; Freundt et al. 2000; Branney and Kokelaar 2002; Dufek et al. 2015; Brand et al. 2023). Most PDCs result from total or partial collapse of an eruptive column, volcanic dome, unstable lava flow front or of an accumulation of pyroclastic material on steep slopes (Druitt 1998; Branney and Kokelaar 2002). Two end-members for the physical regime of PDCs, which often coexist, are described in the literature: dilute turbulent suspensions and dense granular flows with variable amounts of gas pore pressure (Breard et al. 2016; Lube et al. 2020; Brand et al. 2023). Understanding the factors controlling the generation of PDCs, their propagation dynamics and the resulting run-out distance (RD) is a major objective in volcanology due to their potentially devastating consequences both for people and infrastructure (Baxter et al. 1998; Doronzo and Dellino 2011; Cole et al. 2015).

Editorial responsibility: G. A. Valentine

Extended author information available on the last page of the article

Published online: 05 November 2024

Fluidization by gases has long been proposed as one of the main factors controlling PDC propagation (Sparks 1978; Wilson 1980). Fluidization is the result of the differential motion between solid particles and interstitial gas, whose interplay is able to generate pore pressure, counterbalance partially or entirely the solid particle weight, and thus reduce particle friction (Wilson 1980, 1984; Breard et al. 2018; Gravina et al. 2004). In the context of PDCs, fluidization is mainly generated at the impact zone of a collapsing mixture of solid particles and gas (Valentine 2020), while the temporal evolution of fluidization in currents generated from various mechanisms (e.g., dome collapse) is the result of the coupled effect of diffusion, advection, dilatancy, compaction and air entrainment (Iverson and Vallance 2001; Bouchut et al. 2021; Breard et al. 2023). These processes are in turn influenced by the grain-size distribution of the solid particles (Druitt et al. 2007), its variations during flow propagation (Breard et al. 2023), and the underlying topography (Aravena et al. 2021; Brand et al. 2023).

Fluidized granular flows have been largely studied through analogue experiments (Roche et al. 2008; Rowley et al. 2014) which have served as benchmarks for the development and calibration of numerical models (Breard et al. 2019; Aravena et al. 2021). A widely used experimental setup to study granular column collapse is the dam-break configuration (Thompson and Huppert 2007; Roche et al. 2008, 2010; Aravena et al. 2021), which consists in the release of an initially static column of granular material that spreads freely on a flat surface. In this configuration, fluidized granular flows are generated by injecting an air flow through the base of the granular column in order to generate pore pressure and induce fluidization conditions (Roche et al. 2010; Roche 2012). This simple configuration reveals complex feedback mechanisms between pore pressure diffusion and flow propagation, which are thought to be important in nature. For instance, Roche et al. (2008) showed that a slight initial expansion of a few percent of the collapsing granular material is sufficient to confer an inertial fluid-like behaviour to the resulting flow. Roche et al. (2010) described the evolution of the basal pressure during flow propagation and analysed the deposition dynamics of the granular material. Breard et al. (2019) showed by means of a 2D model that pore pressure in granular flows is modulated by dilation and compaction processes, which permitted them to explain the basal pore pressure signals measured in analogue experiments. Aravena et al. (2021) presented a non-depth-averaged model built on the formulation of Chupin et al. (2021) to address the internal dynamics of experimental fluidized granular flows. They considered the temporal evolution of flow front position, run-out distance, thickness of final deposits, sedimentation dynamics, and temporal evolution of pore pressure, showing that the latter could be successfully described considering a constant, effective pore pressure diffusion coefficient (Aravena et al. 2021).

In this study, in order to deepen our understanding of the influence of gas pore pressure on the mobility of PDCs and to obtain constraints to numerically describe these systems and scale results derived from analogue experiments, we adopted the model presented in Aravena et al. (2021, 2022). This model permits us to address the behaviour of collapsing columns with variable aspect ratios (AR) and to test different assumptions to set the effective pore pressure diffusion coefficient under variable setups. With the aim of confirming our model, we compare numerical results with experimental data of dam-break experiments performed using different aspect ratios and fluidization conditions (i.e., fluidized and non-fluidized flows), and we include an analysis on the factors controlling the efficiency of fluidization in facilitating granular material propagation as a function of the length scale of the flow. Finally, we discuss the implications of our results in light of recent advances in our understanding of the influence of fluidization in the transport dynamics of PDCs (Brand et al. 2023; Breard et al. 2019, 2023; Lube et al. 2020; Roche et al. 2021). Note that the new experimental results presented in this paper (in particular, the dependency between aspect ratio and run-out distance for fluidized and non-fluidized granular flows) can be used as reference data to benchmark or validate other numerical models aimed to describe the effect of pore pressure in granular flows and to scale results derived from the analysis of analogue experiments.

Methods

Experimental configuration

The dam-break laboratory experiments presented in this paper were performed with the experimental device described by Roche et al. (2010) (Fig. 1). It includes a reservoir containing a column of granular material, separated by a sluice gate from a 3 m-long, 10 cm-wide horizontal channel where the granular material propagates laterally. The sluice gate device includes a counterweight to ensure a rapid and uniform gate-opening phase. The reservoir base consists of a porous plate, through which a vertical air flow can be injected from below in order to induce fluidization conditions (Roche et al. 2010; Roche 2012). Filters to dry the injected air and a series of manometers are also included in the experimental device in order to control the imposed air flow and ensure the reproducibility of experiments. In the channel, no air flux is provided during flow propagation. The granular material used in the experiments is constituted of spherical glass beads with a density of $\rho_s = 2500$ kg/m^3 and grain size between 60 and 90 μm (mean of 75 μm).

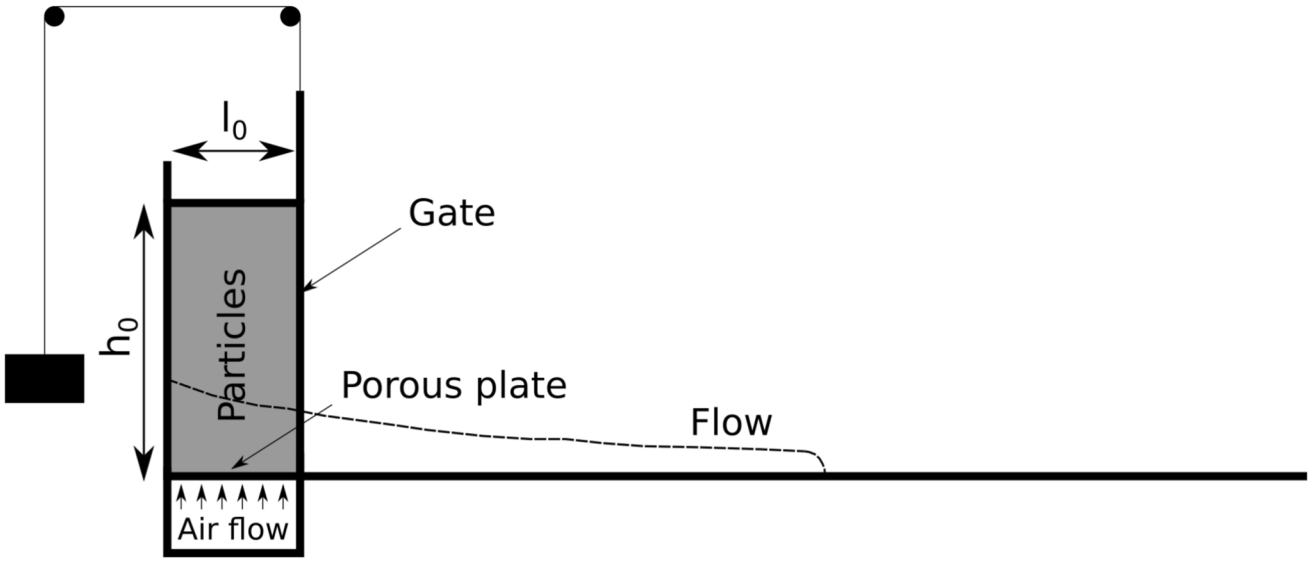

Fig. 1 Simplified scheme of the experimental setup. Modified from Roche et al. (2010)

We performed two sets of experiments (Table 1): (a) non-fluidized flows, where no air flow is imposed on the particle column, and (b) fluidized flows, which are characterised by an air flow supplied from below at a rate equivalent to the *minimum fluidization velocity*, that is, the minimum value that guarantees that the bed weight is counterbalanced by the drag generated by the air flowing between the particles, with the negligible expansion of the granular material. For each set of experiments, we considered variable conditions for collapsing column width (l_0) and column height (h_0), giving rise to aspect ratios (h_0/l_0) between 0.5 and 8.0 (Table 1). Due to experimental limitations, high aspect ratio experiments were only performed with relatively low values of column width (l_0), as given in Table 1. For each experiment, at $t = 0$, the reservoir gate is opened rapidly (< 0.2 s) allowing the granular material to spread laterally (note that air is still injected in the reservoir after gate opening). The resulting deposit is photographed and analysed to obtain the relationship between distance and thickness, and their dependency on flow scale and fluidization conditions.

Table 1 Initial conditions and results of dam-break experiments

Experiment	Inputs			Outputs		
	l_0 [cm]	h_0 [cm]	AR [a]	$\max(h(t_f))$ [b] [cm]	RD [c] [cm]	RD′ [d] [cm]
Non-fluidized						
D1	5	10	2.00	5.2	23.4	15.7
D2	5	20	4.00	7.6	42.9	31.4
D3	5	30	6.00	8.8	60.6	47.0
D4	5	40	8.00	9.5	78.0	62.8
D5	10	10	1.00	8.3	25.8	17.7
D6	10	20	2.00	11.9	55.0	42.0
D7	10	30	3.00	13.9	76.3	61.5
D8	10	40	4.00	15.4	89.9	77.5
D9	15	10	0.67	12.2	24.9	17.1
D10	15	20	1.33	14.7	56.5	43.8
D11	15	30	2.00	17.5	83.8	67.3
D12	15	40	2.67	20.4	102.0	92.7
D13	20	10	0.50	9.9	22.3	16.3
D14	20	20	1.00	16.5	49.6	39.8
D15	20	30	1.50	19.9	81.7	66.6
D16	20	40	2.00	21.8	101.1	85.1

Table 1 continued

Experiment	Inputs			Outputs		
	l_0 [cm]	h_0 [cm]	AR [a]	$\max(h(t_f))$ [b] [cm]	RD [c] [cm]	RD′ [d] [cm]
Fluidized						
F1	5	10	2.00	2.1	35.7	26.0
F2	5	20	4.00	3.0	63.5	53.6
F3	5	30	6.00	3.9	74.6	62.3
F4	5	40	8.00	4.1	90.3	80.2
F5	10	10	1.00	3.2	43.2	30.2
F6	10	20	2.00	4.5	85.2	66.9
F7	10	30	3.00	5.9	100.6	82.9
F8	10	40	4.00	7.8	109.9	92.8
F9	15	10	0.67	4.2	44.9	33.9
F10	15	20	1.33	5.5	106.1	84.9
F11	15	30	2.00	7.6	127.5	107.6
F12	15	40	2.67	8.5	154.6	137.4
F13	20	10	0.50	5.4	41.8	32.1
F14	20	20	1.00	7.1	96.2	74.3
F15	20	30	1.50	8.6	137.6	122.0
F16	20	40	2.00	10.9	153.2	139.5

[a] AR: aspect ratio. [b] $\max(h(t_f))$: maximum thickness of the resulting deposit. [c] RD: run-out distance. [d] RD′: corrected run-out distance, considering a thickness threshold equivalent to the grid dimension used in numerical simulations

Mathematical model

We performed simulations using the mathematical model presented in Aravena et al. (2021). The computational domain Ω is a 2D channel including the reservoir. At any time $t \geq 0$, the computational domain is decomposed as shown in Fig. 2, into $\Omega_s(t)$ which corresponds to the granular mass and $\Omega_f(t)$ which contains only (surrounding) air, called ambient air in the sequel. Note that at $t = 0$, $\Omega_s(t = 0)$ corresponds to the reservoir. The granular phase, in $\Omega_s(t)$, is a mixture of solid particles and air and is described by a two-phase model detailed in Section 2 of Chupin and Dubois (2024). It is based on the conservation of momentum equations for the two phases (Jackson 2000) involving forces between the two components, in particular the drag force which is proportional to the relative velocity. By comparing the order of magnitude of the different terms, the momentum equation of the fluid phase reduces to a simple equation similar to the Darcy law (Chupin and Dubois 2024). As a consequence, the mass conservation equation of the fluid phase leads to

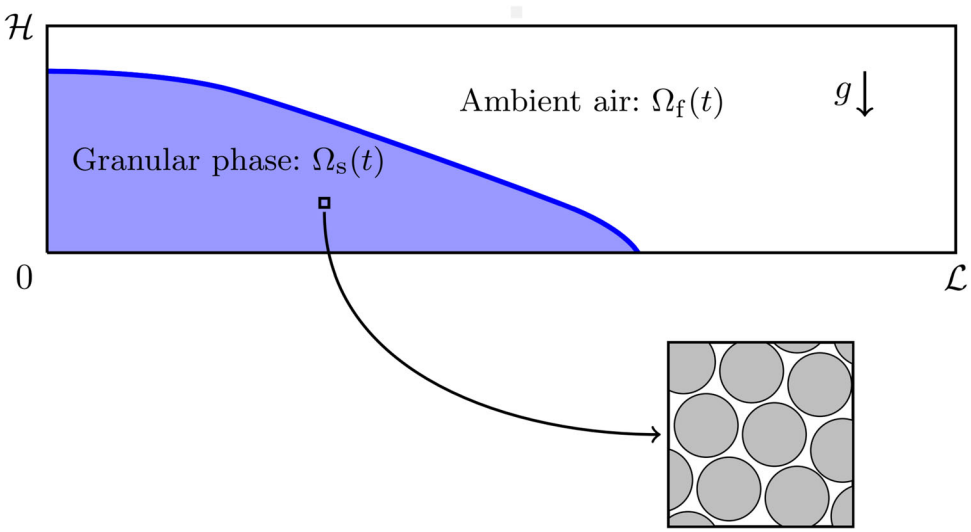

Fig. 2 Computational domain adopted to describe numerically the collapse of a granular column

a linear advection-diffusion equation for the pore pressure (Iverson and Vallance 2001). We assume that the volume fraction of the particles remains constant so that the solid phase is incompressible. Finally, by using the $\mu(I)$ rheology (Jop et al. 2006), the propagation of the granular material is described by the following 2D incompressible model:

$$\phi\rho_s(\partial_t \boldsymbol{u_s} + \boldsymbol{u_s}\cdot\nabla\boldsymbol{u_s}) + \nabla(p_s + p_f) = \phi\rho_s\boldsymbol{g} + \text{div}\,\boldsymbol{T_s} \quad (1)$$

$$\text{div}\,\boldsymbol{u_s} = 0 \quad (2)$$

$$\partial_t p_f + \boldsymbol{u_s}\cdot\nabla p_f = \kappa\Delta p_f \quad (3)$$

where ϕ is the solid particles volume fraction, ρ_s is the solid particles density, $\boldsymbol{u_s}$ is the material velocity, p_s and p_f are the solid (effective) pressure and pore pressure, respectively, $\boldsymbol{g}$ is gravity and κ is the effective pore pressure diffusion coefficient.

The deviatoric stress tensor $\boldsymbol{T_s}$ in Eq. 1 is defined by Jop et al. (2006):

$$\begin{cases} \boldsymbol{T_s} = \mu(I)p_s\frac{\boldsymbol{D(u_s)}}{|\boldsymbol{D(u_s)}|} & \text{if } \boldsymbol{D(u_s)} \neq 0 \\ |\boldsymbol{T_s}| \leq \tan(\alpha)p_s & \text{if } \boldsymbol{D(u_s)} = 0 \end{cases} \quad (4)$$

where $\boldsymbol{D(u_s)} = \frac{1}{2}(\nabla\boldsymbol{u_s} + \nabla\boldsymbol{u_s}^t)$, α is the static internal friction angle of the granular material, and $\mu(I)$ is defined as follows:

$$\mu(I) = \tan(\alpha) + \frac{(\mu_\infty - \tan(\alpha))I}{I + I_0}, \text{ with } I = \frac{2d|\boldsymbol{D(u_s)}|}{\sqrt{p_s/\rho_s}} \quad (5)$$

where μ_∞ is an asymptotic friction coefficient, I_0 is a dimensionless number and d is the diameter of the solid particles.

Following Chupin et al. (2021), the deviatoric stress tensor equation can be rewritten as follows:

$$\boldsymbol{T_s} = 2\eta_s(|\boldsymbol{D(u_s)}|, p_s)\boldsymbol{D(u_s)} + \tan(\alpha)p_s\frac{\boldsymbol{D(u_s)}}{|\boldsymbol{D(u_s)}|} \quad (6)$$

where $\eta_s(|\boldsymbol{D(u_s)}|, p_s)$ is defined by:

$$\eta_s(|\boldsymbol{D(u_s)}|, p_s) = \frac{(\mu_\infty - \tan(\alpha))p_s}{2|\boldsymbol{D(u_s)}| + \frac{I_0}{d}\sqrt{p_s/\rho_s}} \quad (7)$$

Note from this formulation that the granular flow is described by a viscoplastic rheology with viscosity variable in time and space and a Drucker-Prager plasticity criterion (Jop et al. 2006; Ionescu et al. 2015). The numerical scheme adopted in the code includes a projection strategy (Chalayer et al. 2018; Chupin et al. 2021) to treat the singularity of $\boldsymbol{T_s}$ in the absence of strain rate, dispensing with the application of any regularisation technique.

In $\Omega_f(t)$, the ambient gas dynamics (i.e., the air outside the granular flow) is described with Newtonian rheology:

$$\rho_f(\partial_t\boldsymbol{u_f} + \boldsymbol{u_f}\cdot\nabla\boldsymbol{u_f}) + \nabla p_f = \rho_f\boldsymbol{g} + \eta_f\Delta\boldsymbol{u_f} \quad (8)$$

$$\text{div}\,\boldsymbol{u_f} = 0 \quad (9)$$

where ρ_f is air density, $\boldsymbol{u_f}$ is air velocity and η_f is air dynamic viscosity.

Systems of Eqs. 1–3 and 8–9 can be unified by using a level-set formulation (Osher and Fedkiw 2001), which writes:

$$\partial_t\Phi + \boldsymbol{u}\cdot\nabla\Phi = 0 \quad (10)$$

$$\rho(\Phi)(\partial_t\boldsymbol{u} + \boldsymbol{u}\cdot\nabla\boldsymbol{u}) + \nabla(p + p_f) = \rho(\Phi)\boldsymbol{g} + \text{div}\left(2\eta(\Phi)\boldsymbol{D(u)}\right) + \text{div}\,(\tau(\Phi)\boldsymbol{\Sigma}) \quad (11)$$

$$\text{div}\,\boldsymbol{u} = 0 \quad (12)$$

$$\partial_t p_f + \boldsymbol{u}\cdot\nabla p_f = \kappa(\Phi)\Delta p_f \quad (13)$$

where $\boldsymbol{\Sigma}$ is the plastic tensor (see Chupin et al. (2021) for details). The level-set function Φ, which is transported by the velocity field, is used to describe the interface between the granular material and the ambient gas. Initially, the level-set function Φ is defined as the signed distance to the interface ($\Phi < 0$ for the granular flow and $\Phi > 0$ for the ambient gas). A redistancing algorithm is included in the code (Min 2010) and applied periodically in order to keep Φ sufficiently close to the signed distance function. The dependence of density $\rho(\Phi)$, viscosity $\eta(\Phi)$ and yield strength $\tau(\Phi)$ on Φ is given explicitly in Chupin et al. (2021). The diffusion coefficient $\kappa(\Phi)$ is constant and equal to κ in granular material ($\Phi < 0$) and is fixed at 10^{16} m^2/s in air (i.e., where $\Phi > 0$) ensuring that the pore pressure p_f acts only on the granular flow (i.e., $p_f = 0$ where $\Phi > 0$).

Regarding the boundary conditions, Coulomb friction conditions (see Chupin et al. (2021)) with a constant basal friction angle α_b are imposed to the granular flow, while Navier (base), Free (top and reservoir wall), and outflow (wall opposite to the reservoir) boundary conditions are imposed to the air velocity field. Additional details of the model and numerical schemes used to discretise Eqs. 10–13 are given in Chupin et al. (2021) and Aravena et al. (2021, 2022).

Input parameters

As discussed in Aravena et al. (2021), a key model parameter controlling the propagation dynamics of granular flows is the effective pore pressure diffusion coefficient (κ), which determines the rate at which pore pressure (p_f) diffuses within the granular material (see Eq. 3). The benchmarking exercise presented by Aravena et al. (2021) allowed us to constrain the value of κ in the reference experiment (κ = 0.015–0.035

m^2/s), which was performed considering a collapsing column with a height of $h_0 = 40$ cm and a width of $l_0 = 20$ cm, resulting in an aspect ratio of 2.0. However, it is important to highlight that the values of κ obtained from the simulations are one order of magnitude smaller than the theoretical value and that extrapolating our estimates of κ to different aspect ratio collapsing columns is particularly challenging (Montserrat et al. 2012; Aravena et al. 2021). Therefore, we made two assumptions for the present study, which are justified below:

(a) The effective pore pressure diffusion coefficient is independent on flow scale, which is consistent with the theoretical definition of this parameter, i.e., based exclusively on physical properties of the granular material (hydraulic permeability (k), pore volume fraction (ε)), and on viscosity (μ) and compressibility (β) of the interstitial gas. Based on Aravena et al. (2021) and considering the experimental results presented in this work, we consider an effective coefficient $\kappa = 0.025$ m^2/s, and we also included for completeness the theoretical value of κ for the benchmark experiment conditions (i.e., $\kappa = k/(\varepsilon\mu\beta) = 0.130$ m^2/s, for which we have adopted $k \sim 10^{-11}$ m^2, $\varepsilon \sim 0.42$, $\mu \sim 1.8 \cdot 10^{-5}$ Pa s, and $\beta \sim 10^{-5}$ Pa^{-1}).
(b) There is a linear relationship between the effective pore pressure diffusion coefficient and the initial height of the collapsing column (i.e., $\kappa = c \cdot h_0$, where c is a constant parameter). This assumption is consistent with experimental data from static defluidizing columns (Montserrat et al. 2012) but it has not been verified in dam-break experiments yet. Based on the results of Aravena et al. (2021) for the benchmark experiment, we considered $c = 0.0625$ m/s.

Note that both assumptions coincide in the value of κ computed for the benchmark experimental conditions (i.e., $h_0 = 40$ cm and $l_0 = 20$ cm), that is, 0.025 m^2/s. For each assumption, we developed a set of simulations of fluidized flows considering variable collapsing column aspect ratios (ranging from 1 to 8) and a fixed initial column width (l_0) of 20 cm (i.e., as in the benchmark experiment). A complementary set of simulations for non-fluidized granular flows with equivalent geometric characteristics was also performed. Note that, although the variation ranges of aspect ratio are equivalent when compared to our numerical simulations, experimental data of high-aspect-ratio collapsing columns are associated with narrower columns due to limitations to reproduce experimentally collapse processes from too much height. The validity of this comparison scheme is supported by our experimental results of non-dimensional run-out distance as a function of aspect ratio (Fig. 3a), which show a well-defined, continuous dependency pattern between the mentioned variables even when experiments are associated with different values of l_0.

The set of fixed input parameters adopted in our simulations is presented in Table 2. We stress that the inputs of the model (in particular, the Smagorinsky constant and time step) are slightly different from those presented in Aravena et al. (2021) for the benchmark experiment in order to reduce the computational time. These modifications are manifested in differences of the order of 5% in the simulated run-out distances for the benchmark experiment, much smaller than changes associated with the studied variation range of the effective pore pressure diffusion coefficient.

Results

The deposits of experimental fluidized granular flows are characterised by surface slopes that gently decrease downstream, with the maximum thickness observed in the channel near the reservoir (Fig. 4; Roche et al. 2010; Aravena et al. 2021). In contrast, experimental non-fluidized flow deposits present a monotonically decreasing thickness downstream and have significantly larger surface slopes (Fig. 4). The effect of fluidization in increasing the run-out distance is evident in all the tested experimental setups, although the magnitude of this increase is also strongly controlled by the initial collapsing column aspect ratio (Table 1 and Fig. 3a). While fluidization is able to double the run-out distance for aspect ratios of about 1–2, the relative influence of fluidization is significantly reduced for higher aspect ratios. In fact, the non-dimensional run-out distance of fluidized granular flows reaches a peak of about $\sim$ 4–5 for an aspect ratio of $\sim$ 1–2 and then it decreases monotonically and is only slightly larger than that of non-fluidized flows at high aspect ratios (AR $>$ 5). Instead, non-fluidized granular flows present non-dimensional run-out distances weakly controlled by aspect ratio (Fig. 3a), with values around $RD/h_0 = 2$ for the entire variation range of aspect ratio used in experiments, with a relative maximum for aspect ratios of $\sim$ 1–3.

Numerically simulated granular flows present an initial, short acceleration phase followed by a period of flow propagation at nearly constant velocity and finally flow front deceleration and stopping (Fig. 5). Froude numbers computed from numerical simulations during the constant velocity phase are of the order of 0.86–1.59 (non-fluidized flows, with supercritical conditions for AR $>$ 2), 1.21–5.91 (fluidized flows with $\kappa = 0.025$ m^2/s), 1.54–2.69 (fluidized flows with $\kappa = 0.0625$ m/s $\cdot$ h_0) and 1.08–1.95 (fluidized flows with $\kappa = 0.130$ m^2/s). The relative duration of each

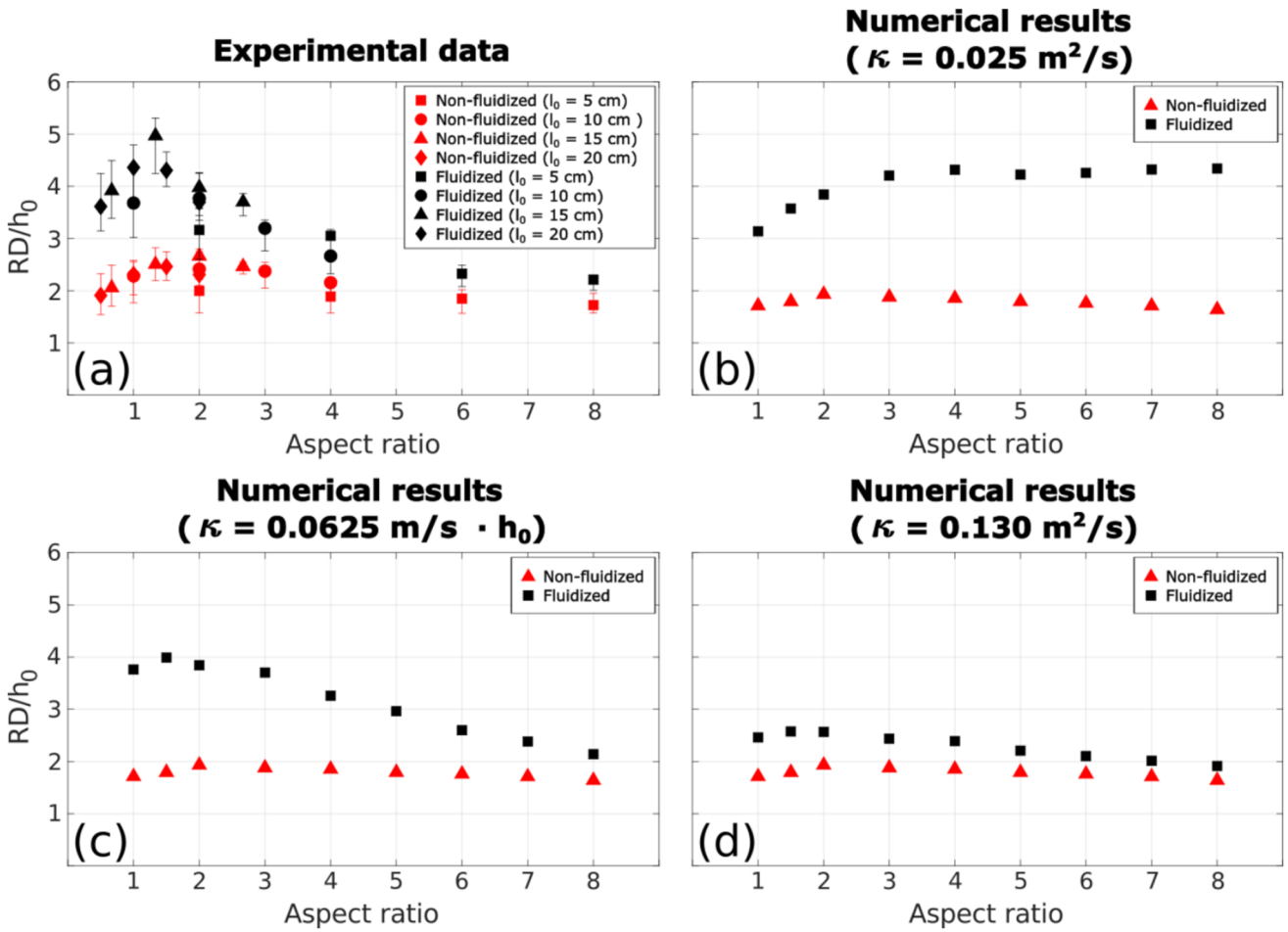

Fig. 3 Non-dimensional run-out distance (RD/h_0) versus aspect ratio for fluidized and non-fluidized dam-break analogue experiments (**a**) and for numerical simulations (**b**, **c**, and **d**), considering different assumptions to set the dependency between the effective pore pressure diffusion coefficient (κ) and collapse height (h_0; see titles). To simplify comparison with numerical results, the experimental data are presented in terms of the observed run-out distance (upper limit of bars) and we also include two corrected values of run-out distance, defined as the distance from the reservoir to the position at which the deposit thickness reaches thresholds equivalent to the cell size used in numerical simulations (lower limit of bars) and equivalent to half the cell size used in numerical simulations (filled markers). Note that the analogue experiments of high-aspect-ratio collapsing columns are associated with lower values of l_0 due to experimental limitations to reproduce collapse processes from too much height

Table 2 Constant input parameters used in numerical simulations

Input parameter	Symbol	Units	Value
Particle density	ρ_s	kg/m^3	2500
Volume fraction of particles in the granular flow [a]	ϕ	–	0.58
Internal friction angle of the granular material	α	°	27
Basal friction angle of the granular material	α_b	°	15
Air density	ρ_f	kg/m^3	1
Air viscosity	η_f	Pa s	$2 \cdot 10^{-5}$
Collapsing column width	l_0	m	0.2
Smagorinsky constant	C_s	–	0.2
Computational cell size	Δx	cm	0.5
Time step	Δt	s	$2 \cdot 10^{-5}$

[a] In non-fluidized simulations, we considered $\phi = 0.62$, which is based on experimental constraints

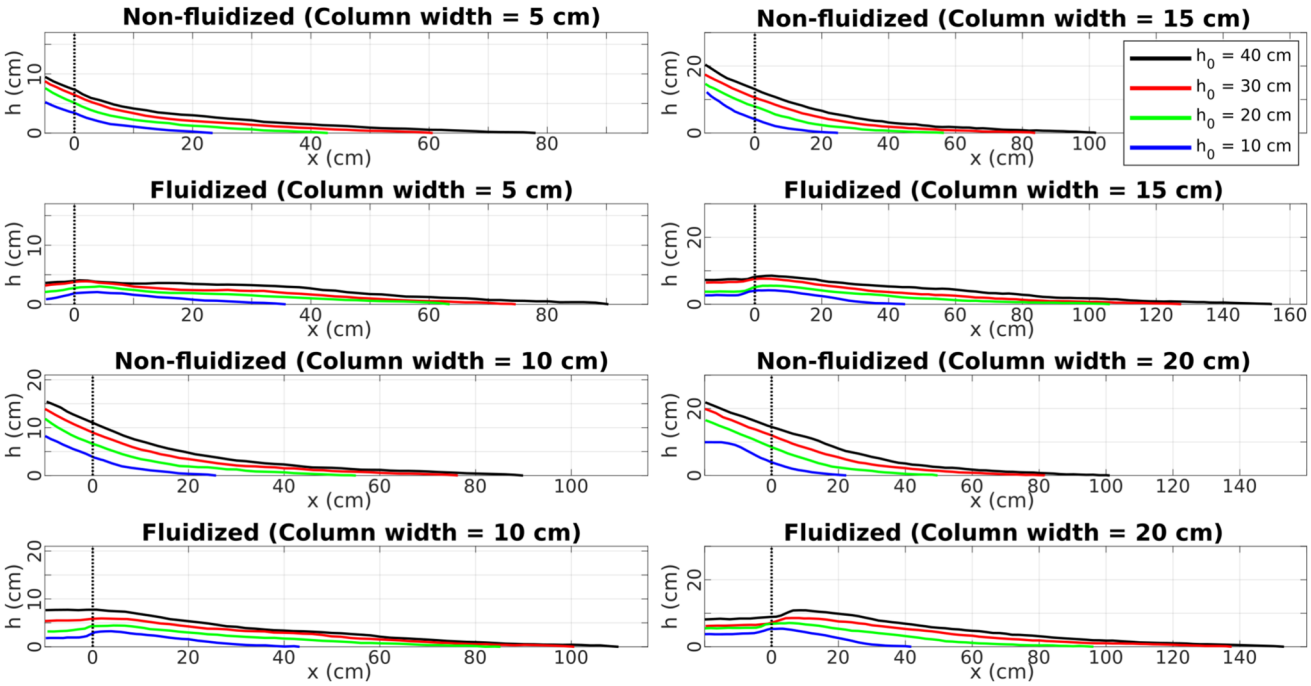

Fig. 4 Surface profiles of deposits for dam-break experiments of fluidized and non-fluidized granular flows (see titles), considering different geometries of the collapsing columns (see legend and titles)

propagation phase is similar in all the simulations presented here, with most of the flow propagation time corresponding to the phase of deceleration (Fig. 6). The significant increase in the non-dimensional run-out distance due to the effect of fluidization is a consequence of the flow dynamics during the early phases of propagation (Fig. 6). In fact, the front acceleration of non-fluidized flows is of the order of $0.7g$, while that of fluidized flows is about $2.0 - 2.3g$. Regarding variations in κ for fluidized flows, they are manifested in differences in the late stage of acceleration and in the duration of the constant front velocity phase (Fig. 6). On the other hand, the rates of deceleration of fluidized and non-fluidized granular flows are remarkably similar ($\sim 0.22g$), regardless of the value of κ. This suggests that initially, fluidized flows behave as non-fluidized flows at late stages of propagation as

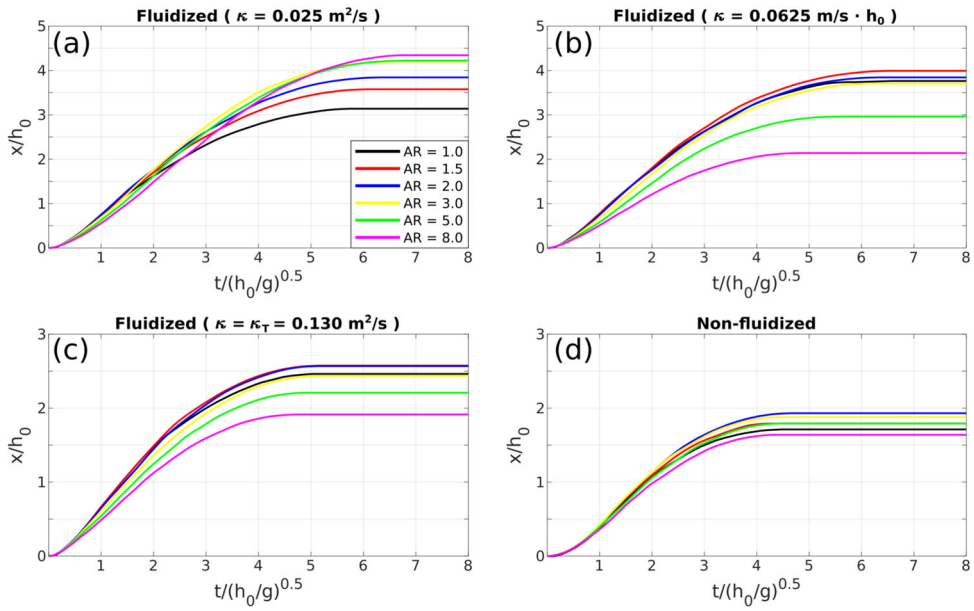

Fig. 5 Non-dimensional position of the flow front as a function of non-dimensional time for numerical simulations of fluidized and non-fluidized granular flows (see titles). Note that numerical results further demonstrate that the theoretical value of κ (**c**) completely fails in predicting the non-dimensional run-out distance measured in analogue experiments (see Fig. 3, i.e., $\mathrm{RD}/h_0 \approx 4$ for an AR of 2.0)

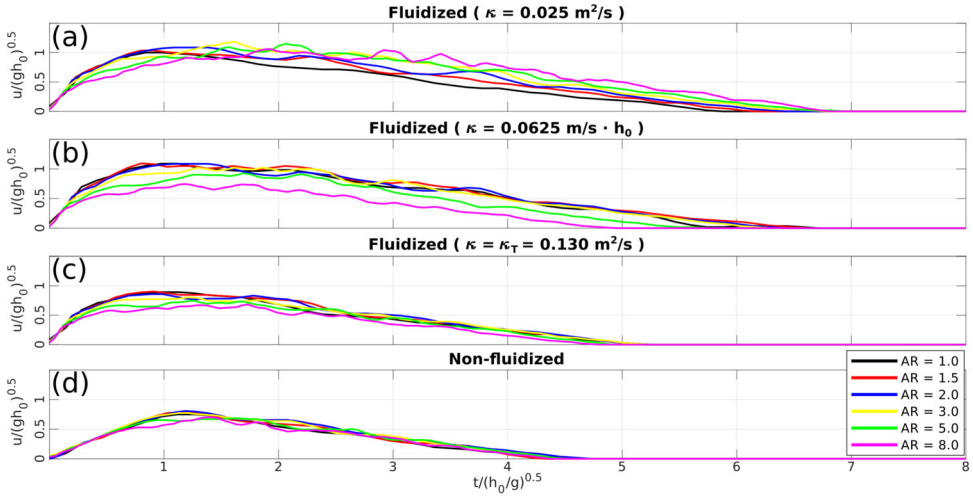

Fig. 6 Non-dimensional velocity of the flow front as a function of non-dimensional time for numerical simulations of fluidized and non-fluidized granular flows (see titles)

a consequence of pore pressure diffusion during flow propagation, as discussed in Aravena et al. (2021).

When κ is assumed independent on flow scale and equal to 0.025 m^2/s (i.e., as determined in Aravena et al. (2021) to fit a benchmark experiment), the simulated non-dimensional run-out distance is an increasing function of aspect ratio up to AR $\approx$ 3 above which it is equal to about 4.2–4.3 (Fig. 3b). Instead, when κ is assumed proportional to h_0, the non-dimensional run-out distance presents a relative maximum for an aspect ratio of about 1.5 and then it decreases rapidly (Fig. 3c). Finally, when κ is assumed equal to the theoretical value (i.e., 0.130 m^2/s), the effect of fluidization in increasing the simulated run-out distance is strongly reduced and a behaviour similar to that of non-fluidized flows is observed (Fig. 3d). The comparison between our simulations and experimental results (Fig. 3a) indicates that a

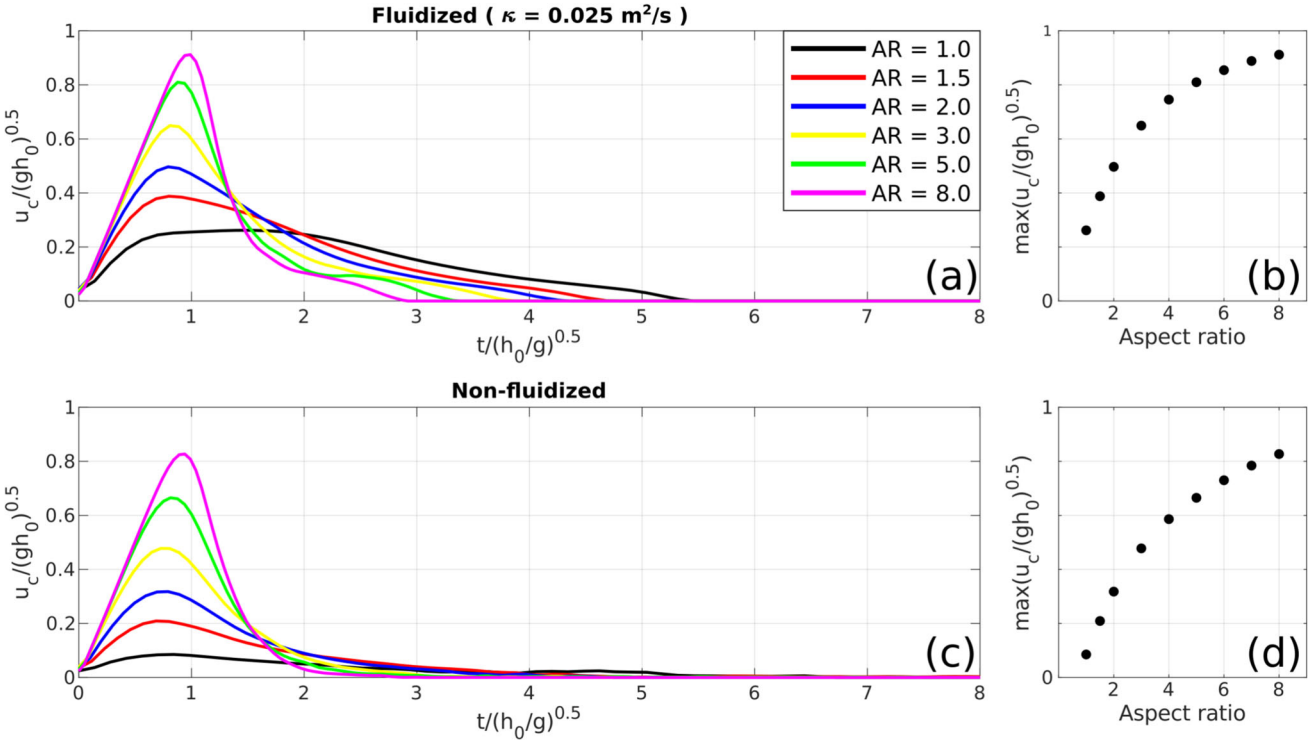

Fig. 7 **a**, **c** Non-dimensional velocity of column collapse in the reservoir as a function of non-dimensional time for numerical simulations of fluidized and non-fluidized granular flows (see titles). **b**, **d** Peak of non-dimensional velocity of column collapse in the reservoir as a function of aspect ratio

positive dependency between the effective pore pressure diffusion coefficient and reservoir column height is needed to describe successfully the behaviour of the studied granular flows. This is also consistent with results for defluidizing static columns (Montserrat et al. 2012) and further demonstrates that the theoretical value of κ fails in predicting the behaviour of the studied analogue experiments of fluidized flows (Figs. 3d and 5c). On the other hand, non-fluidized granular flow simulations present non-dimensional run-out distances weakly controlled by aspect ratio (Fig. 3b, c), with values around 2.0 and a relative maximum at an aspect ratio of $\sim$ 1.5, in fair agreement with experimental data, which further confirm the validity of our model. According to the results described above, the following analysis of our numerical results is focused on non-fluidized flows and on fluidized flows with κ assumed proportional to h_0.

The temporal evolution of the reservoir column collapse velocity for both fluidized and non-fluidized flows is characterised by an initial rapid acceleration phase that lasts about $\sqrt{h_0/g}$ and later a gradual deceleration stage, which is significantly steeper for high-aspect-ratio collapsing columns (Fig. 7). This abrupt reduction in the non-dimensional collapse velocity of high-aspect-ratio collapsing columns limits the rate at which granular material is introduced in the propagation channel and thus the effective influence of fluidization in favoring flow mobility during the final phases of collapse. This effect is enhanced (1) by the decrease of basal pore pressure with time in the reservoir (Fig. 8), which translates into an increase of the friction acting on the granular material during propagation; (2) by the efficient diffusion-driven decrease of pore pressure along the channel, and (3) by the rapidly increasing distance between new arrivals of granular material into the propagation channel and the flow front (Fig. 9). Therefore, the collapsing material at late stages is not able to reach the flow front and to promote the increase of run-out distance, as shown by data in Fig. 3c. Complementary analogue experiments of initially fluidized high-aspect-ratio collapsing columns with stratigraphic markers support this conclusion (Fig. 10). In fact, in these experiments, the granular material reaching the flow front originates from lower levels of the collapsing column. In contrast, the granular material that collapsed during the late stages of the experiments is deposited in proximal to intermediate domains. This observation represents an additional feature of analogue experiments of potential utility for benchmarking numerical models aimed at describing the effect of fluidization in the propagation dynamics of granular flows.

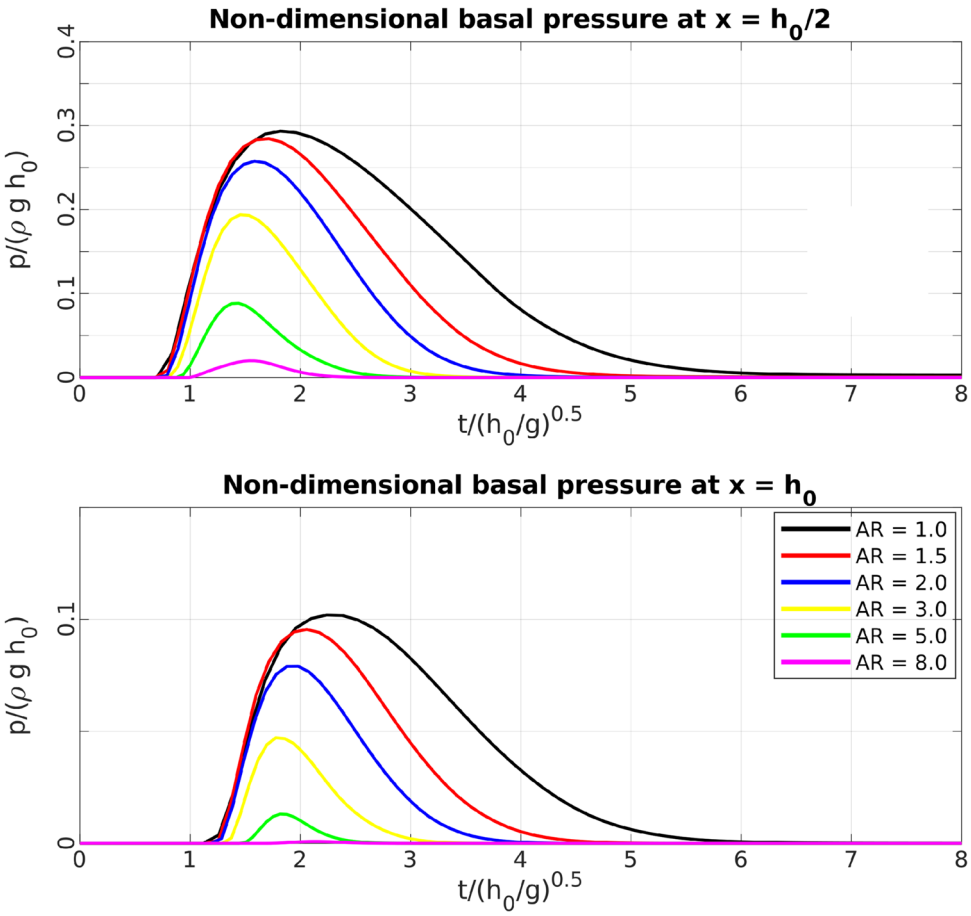

Fig. 8 Temporal evolution of non-dimensional basal pore pressure at two different distances along the channel (see titles) as a function of non-dimensional time for fluidized granular flows (with $\kappa = 0.0625\ \mathrm{m/s} \cdot h_0$), considering different aspect ratio collapsing columns (see legends)

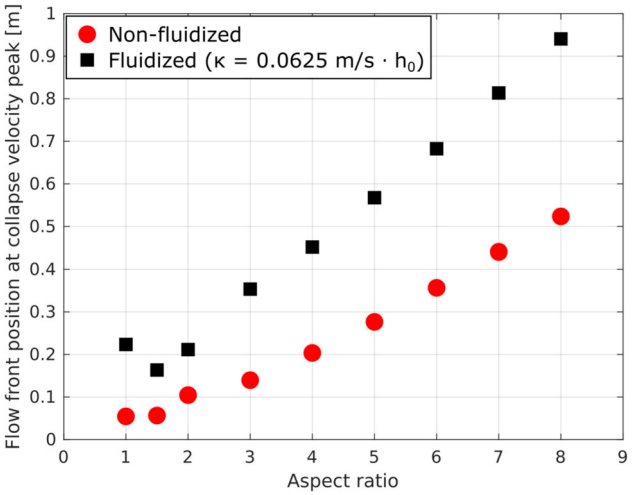

Fig. 9 Flow front position when the peak of collapse velocity is reached as a function of aspect ratio, for simulations of fluidized and non-fluidized granular flows (see legend)

Following Roche (2012); Chupin et al. (2021) and Aravena et al. (2021), we investigated the sedimentation dynamics of granular flows by considering the area of material deposited as a function of time in our numerical simulations (A_d, Fig. 11). To produce results comparable with experiments, we assumed that a given cell of granular material in the computational domain is part of the deposited material if its velocity magnitude was smaller than an arbitrary threshold value of 0.1 m/s, following Aravena et al. (2021). In general, deposition of the granular material occurs at late stages of flow emplacement. For aspect ratios between 3 and 8, most of the deposition occurs during the final 40% of simulations (when the flow has already travelled $>$ 80% of the run-out distance; Fig. 11b, c), while deposition occurs at even later stages of flow propagation ($t/t_f > 0.8$ and $L/L_f > 0.95$; Fig. 11b, c) for collapsing columns with an aspect ratio of about 1. These results

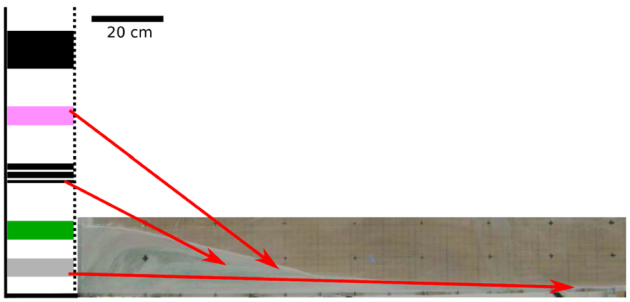

Fig. 10 Results of complementary analogue experiments of an initially fluidized collapsing column, showing that the material reaching the flow front comes from lower levels of the column

are consistent with Roche (2012) and Aravena et al. (2021), and highlight the capability of our model to capture different aspects of granular flows propagation at experimental scale. Note that sedimentation is here described as a consequence of the momentum decrease of solid particles, which differs from other interpretations of sedimentation that consider this process as caused by hindered settling of particles (Girolami and Risso 2020; Shimizu et al. 2023; Roche et al. 2024).

Discussion

In this work, we adopted a 2D multi-phase model to study granular flows in the dam-break configuration, considering in particular high-aspect-ratio collapsing columns. Our simulations permitted us to address how the effect of fluidization in increasing the run-out distance varies with flow dimensions, to analyse the propagation dynamics of fluidized granular flows and to describe sedimentation processes.

Relationship between pore pressure diffusion coefficient and column height

A comparison of numerical results with experimental data suggests that the effective pore pressure diffusion coefficient is an increasing function of the height of the granular material column. This confirms previous observations that the theoretical definition of pore pressure diffusion coefficient does not allow simulation of the behaviour of fluidized granular flows and is consistent with experiments of static defluidizing granular columns (Montserrat et al. 2012; Roche 2012). These experiments, which were performed by measuring the decay in time of basal pore pressure in an initially aerated granular mixture, show a linear relationship between the effective pore pressure diffusion coefficient and reservoir column height. These observations had not been tested in simulations of fluidized granular flows until this study. With the assumption of a linear dependency between κ and h_0, the results of our simulations are close to the experimental data in terms of non-dimensional run-out distance (Fig. 3), even though h_0 can be considered an oversimplified parameter to characterise pore pressure diffusion given that flow height, both in the reservoir and the propagation channel, varies in position and time in dam-break experiments. This agreement between experiments and simulations performed assuming a linear dependency between κ and h_0 could be a consequence of the good correlation recognised in numerical results between h_0 and the average value of flow height in the propagation channel ($\bar{h}$), weighted in time and space by

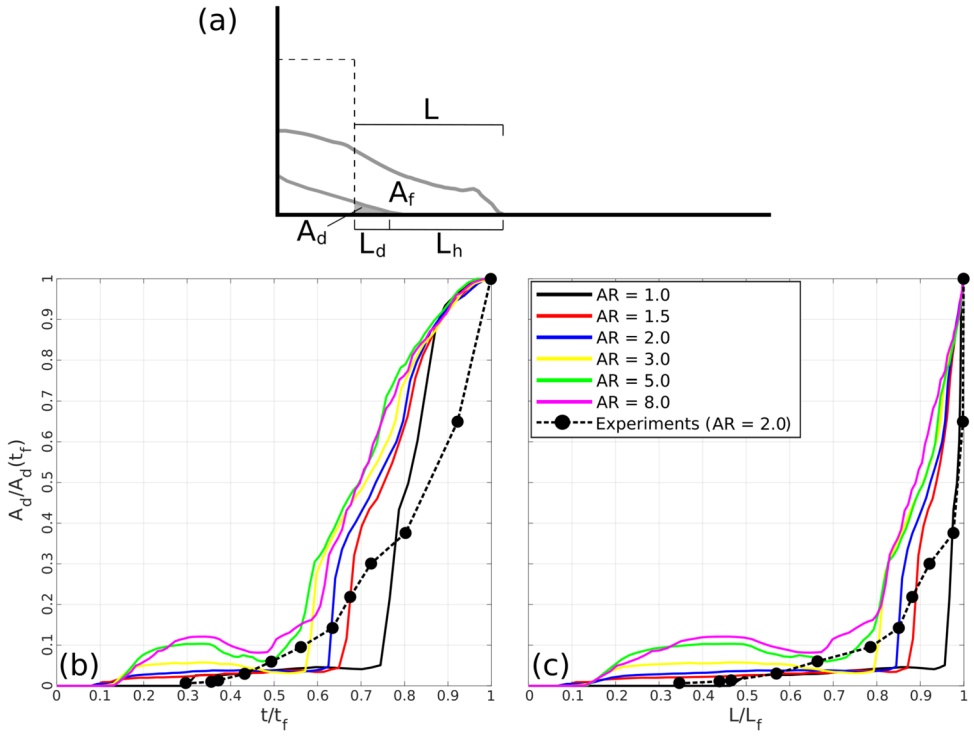

Fig. 11 Deposition dynamics of particles in numerical simulations of fluidized granular flows ($\kappa = 0.0625$ m/s $\cdot h_0$) and experiments. **a** Diagram showing the definitions used to describe the deposition dynamics. A_d: material deposited in the channel. A_f: material flowing. L_d: distance from the reservoir to the sedimentation front. **b** $A_d/A_d(t_f)$ as a function of t/t_f, where t_f is the final time. **c** $A_d/A_d(t_f)$ as a function of L/L_f, where L_f is the final run-out distance

the basal pore pressure as follows:

$$\bar{h} = \frac{\int_0^{l_x} \int_0^{t_f} (h(x,t) \cdot p_f(x, y = 0, t))\, \mathrm{d}t\, \mathrm{d}x}{\int_0^{l_x} \int_0^{t_f} p_f(x, y = 0, t)\, \mathrm{d}t\, \mathrm{d}x}$$

where the horizontal limits of the computational domain are given by $(-l_0)$ and l_x, t_f is the simulation time, $h(x,t)$ is flow height at position x and time t, and $p_f(x, y = 0, t)$ is pore pressure at the base of the propagation channel at position x and time t. The parameter $\bar{h}$ likely represents a more informative parameter to describe the diffusion process of pore pressure in a granular flow. As expected, this results in only small differences among the estimates of κ based on h_0 ($\kappa \propto h_0$) and those based on the parameter $\bar{h}$ ($\kappa \propto \bar{h}$) for the aspect ratio range considered in this study (Fig. 12), which translates in turn into slight variations in the non-dimensional run-out distances derived from the application of both the assumptions to set κ, as shown in Fig. 13. However, please note that $\bar{h}$ is not an input parameter of our model, and thus its use to compute κ involves the application of an iterative procedure that significantly increases the computational time. Moreover, it is worth highlighting that our model considers a constant pore pressure diffusion coefficient, which may not describe correctly the behaviour of fluidized flows due to the effect of dilatancy/compaction (Breard et al. 2019; Bouchut et al. 2021). Based on our results and recent advances in the research field of granular flows (Breard et al. 2019, 2023; Bouchut et al. 2021), we believe that consideration of dilatancy/compaction in future studies based on numerical modelling is crucial to deepen our understanding of the relationship between pore pressure diffusion and flow dimensions.

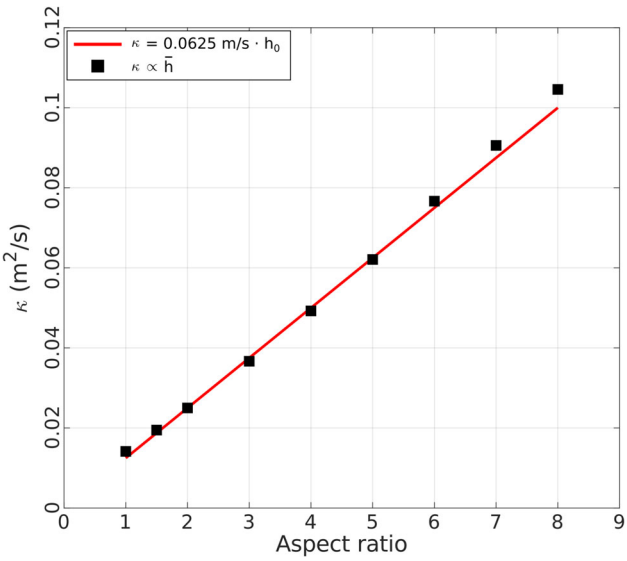

Fig. 12 Effective pore pressure diffusion coefficient as a function of aspect ratio, considering two assumptions to set the dependency between κ and thickness of the granular material: as a function of initial column height (h_0) and as a function of the flow thickness in the channel, weighted in space and time by pore pressure ($\bar{h}$; see legend)

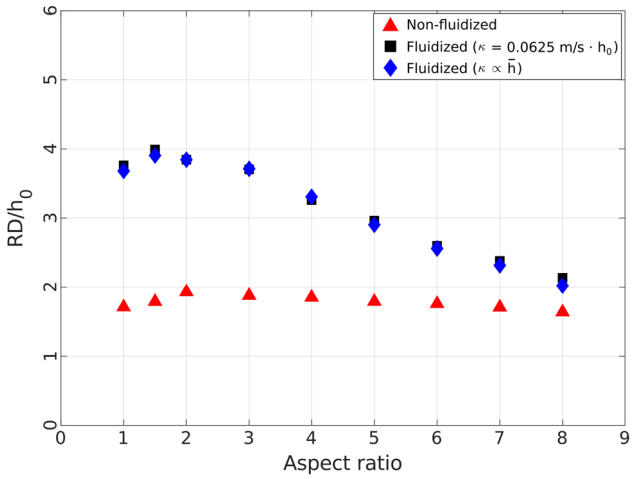

Fig. 13 Non-dimensional run-out distance versus aspect ratio for numerical simulations of fluidized and non-fluidized granular flows, considering different assumptions to set the dependency between κ and thickness of the granular material (see legend)

Efficiency of fluidization in increasing run-out distance and volcanological implications

The analysis of analogue experiments and their numerical description has been widely adopted in volcanology for understanding the dynamics of granular flows such as PDCs (Roche et al. 2010; Roche 2012; Breard et al. 2019; Aravena et al. 2021). However, scaling these results to natural systems is not straightforward and raises still unsolved aspects (Lube et al. 2004, 2005; Delannay et al. 2017; Man et al. 2021). We adopted a numerical modelling-based approach to scale, from a benchmark experimental setup, the behaviour of fluidized granular flows and, from this, we have evaluated the factors controlling the efficiency of fluidization in increasing the mobility of granular flows. We have shown that the interplay between column collapse and flow front velocities determines the relationship between column aspect ratio and run-out distance and that this interplay is critically influenced by initial fluidization. In high-aspect-ratio collapsing columns as those modelled here, the capacity of fluidization to increase the flow run-out distance is hindered by three factors: (1) the abrupt decrease of reservoir column collapse velocity at late stages for high aspect ratios; (2) the rapidly increasing distance between the material entering the propagation channel and the flow front; and (3) the decrease of pore pressure in the reservoir with time and the corresponding increase of friction of the material entering the channel at late stages. Moreover, these factors reinforce the negative feedback mechanism between flow acceleration and fluidization described by Aravena et al. (2021), i.e., that the fluidization-induced velocity increase of the flow reduces its thickness, which in turn promotes rapid pore pressure diffusion and limits the rheological effect of fluidization.

The dam-break configuration can be considered as an analogue of PDCs generated by collapse of lava domes, lava flow fronts or accumulated pyroclastic material. Simulation of initially fluidized conditions applies better to the collapse of pressurised lava domes, and thus our experiments and numerical simulations are expected to be informative of this type of PDCs. The described results show that, in absence of secondary sources of fluidization during granular flow propagation, the positive effect of initial fluidization on non-dimensional run-out distance is maximum for an aspect ratio of 1–2 and it decreases beyond this critical value, suggesting that estimating the initial aspect ratio of a dome susceptible to collapse can be relevant for hazard assessment. Note that our simulations describe the collapse of a homogeneous column characterised by a constant pore pressure diffusion coefficient and uniform density (i.e., incompressibility conditions), while variations in the grain-size distribution and density of the granular material are likely to occur during flow propagation in nature. These variations may induce a more complex dynamics of pore pressure diffusion and thus affect the resulting run-out distance, which is not captured by the presented numerical model. In fact, different authors have addressed the influence of PDC compressibility on pore pressure generation and diffusion (Breard et al. 2019, 2023; Walding et al. 2023). Breard et al. (2019) showed how pore pressure can be modulated by dilation and compaction of granular flows and that, although external sources of gas may enhance the effect of pore pressure in flow mobility, they are not required to generate fluidization conditions in pyroclastic mixtures. Breard et al. (2023) invoke a relevant effect of compressibility and changes in the grain size distribution of the granular mixture during its propagation, which is able to increase the effective pore pressure, reduce basal friction and thus explain the high mobility of some block-and-ash flows. These studies further reinforce the need to incorporate variability in the granular material pore volume and permeability in numerical models aimed at understanding quantitatively the behaviour of pore pressure during the propagation of granular flows and its implications on volcanic hazards.

Concluding remarks

The analysis of dam-break experiments and their numerical simulations, which can be considered as analogues of PDCs generated by the collapse of lava domes, lava flow fronts or accumulated pyroclastic material, reveals that:

(a) The relationship between the timescale of column collapse and that of flow front propagation controls the efficiency of initial fluidization in increasing the run-out distance of granular flows.

(b) In the absence of secondary sources of fluidization and/or significant effects of compressibility/dilatancy during flow propagation, the effect of initial pore pressure of a collapsing column on the non-dimensional run-out distance presents its maximum for aspect ratios between 1 and 2, and this influence decreases rapidly for higher aspect ratios. This is due to the abrupt reduction of collapse velocity recognised in numerical simulations, the decrease of basal pore pressure with time in the reservoir and the rapidly increasing distance between the flow front position and material incorporated into the propagation channel.
(c) Comparison of numerical results with analogue experiments suggests a positive correlation between column height and effective pore pressure diffusion coefficient. This has been previously demonstrated for defluidization of static columns, but this is the first time this relationship is evaluated in dam-break experiments. Further investigation is required to understand the relationship between column height and diffusion coefficient.

Thereby, our study stresses the relevance of having reference experimental data to benchmark and confirm numerical models of granular flows, especially when the physics of these systems is poorly understood and subjected to several sources of uncertainty. We have presented a series of features of fluidized and non-fluidized experimental granular flows that can be potentially useful for the development of benchmarking exercises of numerical models, such as dependency between non-dimensional run-out distance and aspect ratio (Fig. 3); sedimentation dynamics (Fig. 11); and stratigraphic relationship between the collapsing column and the resulting deposit (Fig. 10).

Acknowledgements We thank the editor and reviewers of this manuscript, Dr. Greg Valentine, Dr. Eric Breard, and Dr. Hiroyuki Shimizu, for their valuable contributions and suggestions, which significantly improved this paper.

Funding This research was financed by the French government IDEX-ISITE initiative 16-IDEX-0001 (CAP 20–25). This is Laboratory of Excellence ClerVolc contribution number 669. The numerical simulations have been performed on a DELL cluster with 32 processors Xeon E2650v2 (8 cores), 1 To of total memory, and an infiniband (FDR 56Gb/s) connecting network. This cluster has been financed by the French Government Laboratory of Excellence initiative n°ANR-10-LABX-0006. Alvaro Aravena has been supported by the Millennium Institute on Volcanic Risk Research - Ckelar Volcanoes ANID/MILENIO (grant no. ICN2021_038).

References

Aravena A, Chupin L, Dubois T, Roche O (2021) The influence of gas pore pressure in dense granular flows: numerical simulations versus experiments and implications for pyroclastic density currents. Bull Volcanol 83(11):1–20

Aravena A, Chupin L, Dubois T, Roche O (2022) Fluidization by pore pressure of dense granular flows: numerical simulations versus experiments. In: 8th European Congress on Computational Methods in Applied Sciences and Engineering (ECCOMAS 2022)

Baxter PJ, Neri A, Todesco M (1998) Physical modelling and human survival in pyroclastic flows. Nat Hazards 17:163–176

Bouchut F, Fernández-Nieto ED, Koné EH, Mangeney A, Narbona-Reina G (2021) Dilatancy in dry granular flows with a compressible μ(i) rheology. J Comput Phys 429:110013

Brand BD, Pollock N, Vallance JW, Esposti Ongaro T, Roche O, Trolese M, Giordano G, Marshall AA, Criswell CW (2023) Advances in our understanding of pyroclastic current behavior from the 1980 eruption sequence of Mount St. Helens volcano (Washington), USA. Bulletin of Volcanology 85(4):24

Branney M, Kokelaar P (2002) Pyroclastic density currents and the sedimentation of ignimbrites. Geological Society of London, London

Breard E, Lube G, Jones J, Dufek J, Cronin S, Valentine G, Moebis A (2016) Coupling of turbulent and non-turbulent flow regimes within pyroclastic density currents. Nat Geosci 9(10):767–771

Breard E, Dufek J, Lube G (2018) Enhanced mobility in concentrated pyroclastic density currents: an examination of a self-fluidization mechanism. Geophys Res Lett 45(2):654–664

Breard E, Dufek J, Roche O (2019) Continuum modeling of pressure-balanced and fluidized granular flows in 2-D: comparison with glass bead experiments and implications for concentrated pyroclastic density currents. Journal of Geophysical Research: Solid Earth 124(6):5557–5583

Breard EC, Dufek J, Charbonnier S, Gueugneau V, Giachetti T, Walsh B (2023) The fragmentation-induced fluidisation of pyroclastic density currents. Nat Commun 14(1):2079

Chalayer R, Chupin L, Dubois T (2018) A bi-projection method for incompressible bingham flows with variable density, viscosity, and yield stress. SIAM J Numer Anal 56(4):2461–2483

Chupin L, Dubois T (2024) Non-isochoric stable granular models taking into account fluidisation by pore gas pressure. J Fluid Mech 979:A14

Chupin L, Dubois T, Phan M, Roche O (2021) Pressure-dependent threshold in a granular flow: numerical modeling and experimental validation. J Nonnewton Fluid Mech 291

Cole P, Neri A, Baxter P (2015) Hazards from pyroclastic density currents. The Encyclopedia of Volcanoes. Academic Press, New York, pp 943–956

Delannay R, Valance A, Mangeney A, Roche O, Richard P (2017) Granular and particle-laden flows: from laboratory experiments to field observations. J Phys D Appl Phys 50(5):053001

Doronzo DM, Dellino P (2011) Interaction between pyroclastic density currents and buildings: numerical simulation and first experiments. Earth Planet Sci Lett 310(3–4):286–292

Druitt T (1998) Pyroclastic density currents. Geological Society, London, Special Publications 145(1):145–182

Druitt TH, Avard G, Bruni G, Lettieri P, Maez F (2007) Gas retention in fine-grained pyroclastic flow materials at high temperatures. Bull Volcanol 69(8):881–901

Dufek J, Esposti Ongaro T, Roche O (2015) Pyroclastic density currents: processes and models. In: The Encyclopedia of Volcanoes. Academic Press, New York

Freundt A, Wilson C, Carey S (2000) Ignimbrites and block-and-ash flow deposits. In: The Encyclopedia of Volcanoes. Academic Press, New York

Girolami L, Risso F (2020) Physical modeling of the dam-break flow of sedimenting suspensions. Physical Review Fluids 5(8):084306

Gravina T, Lirer L, Marzocchella A, Petrosino P, Salatino P (2004) Fluidization and attrition of pyroclastic granular solids. J Volcanol Geoth Res 138(1–2):27–42

Ionescu IR, Mangeney A, Bouchut F, Roche O (2015) Viscoplastic modeling of granular column collapse with pressure-dependent rheology. J Nonnewton Fluid Mech 219:1–18
Iverson RM, Vallance JW (2001) New views of granular mass flows. Geology 29(2):115–118
Jackson R (2000) The dynamics of fluidized particles. Cambridge University Press
Jop P, Forterre Y, Pouliquen O (2006) A rheology for dense granular flows. Nature 441:727–730
Lube G, Huppert HE, Sparks RSJ, Hallworth MA (2004) Axisymmetric collapses of granular columns. J Fluid Mech 508:175–199
Lube G, Huppert HE, Sparks RSJ, Freundt A (2005) Collapses of two-dimensional granular columns. Phys Rev E 72(4):041301
Lube G, Breard E, Esposti Ongaro T, Dufek J, Brand B (2020) Multiphase flow behaviour and hazard prediction of pyroclastic density currents. Nature Reviews Earth & Environment 1(7):348–365
Man T, Huppert HE, Li L, Galindo-Torres SA (2021) Finite-size analysis of the collapse of dry granular columns. Geophysical Research Letters 48(24):e2021GL096054
Min C (2010) On reinitializing level set functions. J Comput Phys 229(8):2764–2772
Montserrat S, Tamburrino A, Roche O, Niño Y (2012) Pore fluid pressure diffusion in defluidizing granular columns. Journal of Geophysical Research: Earth Surface 117(F2)
Osher S, Fedkiw RP (2001) Level set methods: an overview and some recent results. J Comput Phys 169(2):463–502
Roche O (2012) Depositional processes and gas pore pressure in pyroclastic flows: an experimental perspective. Bull Volcanol 74(8):1807–1820
Roche O, Montserrat S, Niño Y, Tamburrino A (2008) Experimental observations of water-like behavior of initially fluidized, dam break granular flows and their relevance for the propagation of ash-rich pyroclastic flows. Journal of Geophysical Research: Solid Earth 113(B12)
Roche O, Montserrat S, Niño Y, Tamburrino A (2010) Pore fluid pressure and internal kinematics of gravitational laboratory air-particle flows: insights into the emplacement dynamics of pyroclastic flows. Journal of Geophysical Research: Solid Earth 115(B9)
Roche O, Azzaoui N, Guillin A (2021) Discharge rate of explosive volcanic eruption controls runout distance of pyroclastic density currents. Earth Planet Sci Lett 568:117017
Roche O, Azzaoui N, Guillin A (2024) Different physics but similar dependence of runout distance with discharge rate: the duality of pyroclastic density currents. Bull Volcanol 86(7):65
Rowley PJ, Roche O, Druitt TH, Cas R (2014) Experimental study of dense pyroclastic density currents using sustained, gas-fluidized granular flows. Bull Volcanol 76(9):1–13
Shimizu HA, Koyaguchi T, Suzuki YJ (2023) Dynamics and deposits of pyroclastic density currents in magmatic and phreatomagmatic eruptions revealed by a two-layer depth-averaged model. Geophysical Research Letters 50(16):e2023GL104616
Sparks R (1978) Gas release rates from pyroclastic flows: a assessment of the role of fluidisation in their emplacement. Bulletin Volcanologique 41:1–9
Thompson EL, Huppert HE (2007) Granular column collapses: further experimental results. J Fluid Mech 575:177–186
Valentine GA (2020) Initiation of dilute and concentrated pyroclastic currents from collapsing mixtures and origin of their proximal deposits. Bull Volcanol 82(2):1–24
Walding N, Williams R, Rowley P, Dowey N (2023) Cohesional behaviours in pyroclastic material and the implications for deposit architecture. Bull Volcanol 85(11):67
Wilson C (1980) The role of fluidization in the emplacement of pyroclastic claws: an experimental approach. J Volcanol Geoth Res 8(2–4):231–249
Wilson C (1984) The role of fluidization in the emplacement of pyroclastic flows, 2: experimental results and their interpretation. J Volcanol Geoth Res 20(1–2):55–84

Authors and Affiliations

Alvaro Aravena[1,2,3] · Laurent Chupin[4] · Thierry Dubois[4] · Olivier Roche[2]

✉ Alvaro Aravena
aaravena@ucm.cl

Laurent Chupin
laurent.chupin@uca.fr

Thierry Dubois
thierry.dubois@uca.fr

Olivier Roche
olivier.roche@uca.fr

[1] Facultad de Ciencias Básicas, Universidad Católica del Maule, Av. San Miguel 3605, Talca, Chile

[2] Laboratoire Magmas et Volcans, Université Clermont Auvergne, CNRS, IRD, OPGC, 6 Avenue Blaise Pascal, Clermont-Ferrand, France

[3] Millennium Institute on Volcanic Risk Research - Ckelar Volcanoes, Avenida Angamos 0610, Antofagasta, Chile

[4] Laboratoire de Mathématiques Blaise Pascal, Université Clermont Auvergne, CNRS, 3 Place Vasarely, Clermont-Ferrand, France